Analysis of microRNA expression profiles in exosomes derived from acute myeloid leukemia by p62 knockdown and effect on angiogenesis

Chuan Li[1,*], Xinyi Long[1,*], Peiqi Liang[2], Zhuogang Liu[1], Chen Wang[1] and Rong Hu[1]

[1] Hematology Department, Shengjing Hospital of China Medical University, Shenyang, China
[2] Hematology Department, The First Affiliated Hospital of Suzhou University, Suzhou, China
[*] These authors contributed equally to this work.

ABSTRACT

Objectives. In this study, we aimed to investigate the effect of p62 on angiogenesis and microRNA (miRNA) expression profiles in acute myeloid leukemia (AML) exosomes.
Methods. An Exiqon v19.0 microRNA MicroArray was used to profile miRNAs in exosomes derived from parental and p62-knockdown U937 cells. The Gene Ontology (GO) and Kyoto Encyclopedia of Genes and Genomes (KEGG) databases were used to predict the biological functions and potential mechanisms of differentially expressed miRNAs in AML exosomes. Endothelial cell tube formation assays using human umbilical vein endothelial cells (HUVECs) were performed to investigate the effect of AML exosomes on angiogenesis.
Results. We demonstrated that 2,080 miRNAs were expressed in exosomes derived from our cultured cell samples, of which 215 and 208 miRNAs were upregulated and downregulated, respectively, in p62-knockdown U937 cells (fold change ≥ 2, $P < 0.05$). GO analysis indicated that miRNAs were most enriched in the intercellular pathways. Biological process analysis revealed that 1460 biological processes were associated with downregulated transcripts, including 19 pathways related to vesicles, and 1,515 pathways were upregulated, including 8 pathways related to vesicles. Molecular function analysis indicated that protein binding, transcription regulator activity, and DNA-binding transcription factor activity were enriched ($P < 0.05$). Pathway analysis indicated that 84 pathways corresponded to upregulated transcripts, and 55 pathways corresponded to downregulated transcripts ($P < 0.05$). We also found that exosomes derived from U937 cells promoted angiogenesis in HUVECs.
Conclusions. Our data suggest that exosomal miRNAs may play important roles in the pathogenesis of AML, which may be treated by p62 knockdown with exosomal miRNAs to inhibit angiogenesis.

Subjects Biochemistry, Bioinformatics, Cell Biology, Molecular Biology, Translational Medicine
Keywords Exosome, microRNA, Acute myeloid leukemia, P62, Angiogenesis

Submitted 3 January 2022
Accepted 5 May 2022
Published 22 July 2022

Corresponding author
Rong Hu, hur@sj-hospital.org

Academic editor
Vladimir Uversky

Additional Information and Declarations can be found on page 15

DOI **10.7717/peerj.13498**

How to cite this article Li C, Long X, Liang P, Liu Z, Wang C, Hu R. 2022. Analysis of microRNA expression profiles in exosomes derived from acute myeloid leukemia by p62 knockdown and effect on angiogenesis. *PeerJ* **10**:e13498 http://doi.org/10.7717/peerj.13498

INTRODUCTION

Acute myeloid leukemia (AML) is a fatal hematological malignancy with high recurrence rate. For patients receiving the most intensive treatment, the overall 5-year survival rate remains below 50%. For the remaining patients, the prognosis is even worse (*Burnett, Wetzler & Lowenberg, 2011*). AML is characterized by multiple recurring mutations. These mutations affect disease response to treatment and the risk of recurrence (*Patel et al., 2012*; *Short, Rytting & Cortes, 2018*; *Staudt et al., 2018*; *Xie et al., 2014*). P62 regulates cell survival and death via various signal transduction pathways (*Komatsu, Kageyama & Ichimura, 2012*). A study found that upregulated p62 expression could promote AML cell maturation into granulocytes, depending on NF-κB activation, predicting poor AML prognosis (*Trocoli et al., 2014*). In addition, loss of p62 impaired leukemia cell growth and colony formation and prolonged the development of leukemia in mice (*Nguyen et al., 2019*). High expression of the selective autophagy receptor p62 is associated with a poor prognosis in AML (*Nguyen et al., 2019*).

Exosomes are nanometer-scale extracellular vesicles containing many microRNAs (miRNAs) that are secreted from cells in both normal and pathological conditions (*Skog et al., 2008*). It has been found that normal hematopoietic stem cell proliferation and differentiation are suppressed by exosomes releasing miR-150 and miR-155 through c-MYB inhibition. In this manner, a malignant phenotype constitutes perpetual existence by changing hematopoietic stem cell biological behaviors (*Hornick et al., 2016*). This finding suggests a biological role for such miRNAs in malignant tumor progression (*De Kouchkovsky & Abdul-Hay, 2016*). Leukemic cells can stimulate neovascularization in the bone marrow (*Wang et al., 2019*) and secrete angiogenic factors, indicating adverse prognosis in AML (*Haouas, 2014*). Exosomes may accelerate angiogenesis and promote tumor progression by harboring miRNAs (*Aslan et al., 2019*). Thus, exosomal miRNAs may be new targets for AML treatment. However, regulation of angiogenesis by p62 remains largely unknown.

In this study, we constructed a miRCURYTM LNA Array (v.19.0) of miRNAs in exosomes derived from AML cells after p62 knockdown. The miRNAs in exosomes were analyzed by identifying signature miRNAs. We then investigated angiogenesis in human umbilical vein endothelial cells (HUVECs) exposed to exosomes derived from parental U937 cells, p62-knockdown U937 cells, or control cells. The data from these studies may shed light on the relationship between exosomal miRNAs and AML, further enhancing our understanding of AML progression.Our study may aid the development of potential biomarkers for the diagnosis and prognosis of AML progression.

MATERIALS AND METHODS

Cell culture and lentiviral vector cell line construction

The human acute monocytic leukemia cell line U937 was purchased from the Bena Culture Collection (Beijing, China) and stored in our laboratory. A recombinant lentivirus vector-mediated *SQSTM1* gene (LV-SQSTM1-RNAi) and an empty recombinant adenovirus vector (Hu6-MCS-CMV-EGFP) were constructed. U937 cells were placed in a six-well

plate. Polybrene (Gene, Shanghai, China) was used for the transfection. The transfection system included 1.8 mL RPMI-1640 with 10% fetal bovine serum, 10 μL LV-SQSTM1-RNAi or Hu6-MCS-CMV-EGFP, and 0.9 μL polybrene. After transfection for 24 h, the cell suspension was collected and centrifuged at 800 rpm for 5 min, the supernatant was discarded, and two mL of RPMI-1640 with 10% fetal bovine serum was added. After transfection for 48 h, fluorescence was observed. After culturing, 5 μg/mL puromycin was added, and the cells were screened for 15 days. After selecting the surviving cells, cell lines with clonal stability were cryopreserved and characterized through RT–qPCR and western blotting.

Cell viability cell counting kit (CCK)-8

U937 cells were plated at a density of 3–5 $\times$ 10^4 cells/well in 96-well plates and allowed to grow for 12, 24, and 48 h. Next, 10 μL CCK-8 solution (Promega, Madison, WI, USA) was added to the cell suspension and incubated for 2 h. Absorbance was measured using a spectrophotometer at 450 nm. The experiment was repeated at least three times.

Flow cytometric cell apoptosis

Flow cytometry analysis using an Annexin V-FITC/PI detection kit was used to compare the apoptosis rate of p62-control and p62 knockdown U937 cells. After 48 h of incubation, the cells were washed with phosphate-buffered saline and resuspended in 400 μL of 1$\times$ binding buffer. Thereafter, 5 μL Annexin V-FITC and 5 μL PI were added to the mixture and stained in the dark for 15 min at room temperature. Apoptosis was detected using flow cytometry (Beckman Coulter, La Brea, CA, USA) immediately after staining.

Exosome collection and identification

P62-siRNA coated with lentivirus interfered with U937 cells to downregulate the expression of p62, with the empty virus vector used as a control. Two groups of cells were used as follows: p62-knockdown U937 cells and controls. The two groups of cells were cultured for 48 h in serum-free media. The supernatant was collected for exosome extraction via ultracentrifugation. Exosome shape and size were observed using electron microscopy, and exosomal markers were detected using western blot analysis.

Western blot analysis

Total protein was extracted from U937 cells that had or had not been transfected with the p62-encoding gene using radioimmunoprecipitation assay lysis buffer (Beyotime, Shanghai, China). The protein concentration was determined using the BCA method. Equal amounts of protein samples were added to each well, separated using 10% SDS-PAGE, and transferred to a polyvinylidene chloride transfer membrane (Merck Millipore, Burlington, MA, USA). The membrane was blocked with 5% skimmed milk for 2 h. It was then washed with TBST and incubated with primary antibodies against p62, TSG101, CD63, CD9, calnexin, and GAPDH (all from Abcam, Cambridge, UK; 1:1000) overnight at 4 °C. Thereafter, the membrane was incubated with anti-rabbit or anti-mouse horseradish peroxidase-conjugated secondary antibodies at room temperature for 2 h after washing three times with TBST. An enhanced chemiluminescence substrate (Thermo Fisher

Scientific) was used to detect the protein bands. Image Lab software was used to detect and analyze the density of each band (Bio-Rad, Hercules, CA, USA).

RNA extraction, miRNA labeling and array hybridization

TRIzol (Invitrogen, Carlsbad, CA, USA) was used to extract total RNA. A NanoDrop spectrophotometer (ND-1000; NanoDrop Technologies, Wilmington, DE, USA) was used to measure RNA quality and quantity. RNA integrity was assessed using gel electrophoresis. After quality control, miRNA labeling was performed according to the instructions of the miRCURY^{TM} Hy3^{TM}/Hy5^{TM} Power Labeling Kit (Exiqon, Vedbaek, Denmark). First, 1 μL RNA in 2 μL water was mixed with 1 μL CIP buffer and CIP (Exiqon, Vedbaek, Denmark). The mixture was then incubated at 37 °C for 30 min. The mixture was incubated at 95 °C for 5 min to stop the reaction. Then, 3 μL labeling buffer, 1.5 μL fluorescent label (Hy3TM), 2 μL dimethyl sulfoxide, and 2 μL labeling enzyme were added. The mixture was then incubated for 1 h at 16 °C, followed by 15 min at 65 °C to terminate the reaction. Hy3-labeled samples were hybridized on the miRCURYTM LNA array (v.19.0; Exiqon, Vedbaek, Denmark) according to the manufacturer's instructions. A total of 25 μL Hy3^{TM}-labeled samples and 25 μL hybridization buffer were denatured at 95 °C for 2 min and then incubated on ice for 2 min. The hybridization system (Nimblegen Systems, Inc., Madison, WI, USA) was used with the microarray set at 56 °C for 16 to 20 h. After hybridization, the slides were washed several times using a washing buffer kit (Exiqon, Vedbaek, Denmark). Finally, an Axon GenePix 4000 B microarray scanner (Axon Instruments, Foster City, CA, USA) was used to scan the slides.

miRNA array scanning and analysis

GenePix Pro 6.0 software (Axon, Instruments, Foster City, CA, USA) was used to extract data by analyzing the imported scanned images. The samples were chosen to calculate normalization factors if the replicated miRNAs were averaged and for miRNAs with intensities $\geq$30. Median normalization was used to normalize the data. Normalized data = (foreground background)/median; the median was the 50% quantile of miRNA intensity, which was larger than 30 in all samples after background correction. After normalization, the miRNAs with significant differences between the two groups were determined according to the fold change and *P* value. Finally, hierarchical clustering was used to show the different miRNA expression profiles between the samples.

MiRNA and mRNA networks and prediction of miRNA function

TargetScan7.1 (http://www.targetscan.org/) and mirdbV5 (http://mirdb.org/) are online sites for miRNA target gene prediction (*Agarwal et al., 2015*; *Chen & Wang, 2020*). In our research, we used two databases to predict the target genes of differentially expressed miRNAs: targetscan7.1 and mirdbV5.

Gene ontology (GO) and kyoto encyclopedia of genes and genomes (KEGG) pathway analyses of differentially expressed miRNAs

We used the GO (http://www.geneontology.org) and KEGG (http://www.genome.ad.jp/kegg/) databases to study the potential organisms and signaling pathways of differentially expressed miRNAs. Differences were considered statistically significant at $P < 0.05$.

Endothelial cell tube formation assays

HUVECs were exposed to exosomes derived from parental U937 cells, p62-knockdown U937 cells, or p62-control cells when cultured in 1640 medium. Cells were plated in 96-well plates with 50 μL Matrigel (BD Biosciences), seeded at 3 × 104 cells per well. Tubules were photographed using phase microscopy after incubation for 0, 3, and 6 h at 37 °C with 5% CO2.

Statistical analysis

We used GraphPad Prism 6 to corroborate the statistical significance of the data for all graphs in this study. Values are presented as the means ± standard deviation. Differences between groups were analyzed using Student's *t*-test, and statistical significance was set at $P < 0.05$.

RESULTS

Confirmation of knockdown p62 in U937 cell line

To generate p62-knockdown U937 cells, we used a lentivirus to transfect cells and observed the transfection efficiency by fluorescence microscopy. We then conducted RT–qPCR analysis to determine the expression levels of the autophagy gene encoding p62 (Figs. 1A–1B) and western blotting to detect the expression levels of the autophagy core protein p62 (Figs. 1C–1D). Notably, we found that the p62 gene and protein expression levels in U937 cells were successfully reduced compared with controls after LV-SQSTM1-RNAi treatment. CCK8 (Fig. 1E), and flow cytometry (Figs. 1F–1G), show that p62 knockdown inhibits the proliferation of U-937 cells and promotes apoptosis.

Characteristics of exosomes

We observed exosome formation using electron microscopy after ultracentrifugation. Electron microscopy revealed exosomes as vesicles with a double-layer membrane structure (30–100 nm in diameter, Fig. 2A). Western blotting indicated that exosomes expressed TSG101, CD63, and CD9, but not calnexin (Fig. 2B). Exosome concentrations and quantities were measured using BCA. The concentrations of parental, control, and p62-knockdown U937 cells were 2.248 ± 0.245, 2.212 ± 0.092, and 2.189 ± 0.102, respectively (Figs. 2C, 2D). We found that the quantity of exosomes in p62-knockdown U937 cells was lower than that in the controls ($P < 0.05$).

Differentially expressed miRNAs in exosomes and PCR verification

We chose differentially expressed miRNAs in exosomes based on the fold change in the two samples. Microarray analysis revealed that 2,080 miRNAs were expressed in exosomes, 215 were upregulated, and 208 were downregulated (fold change ≥ 2, $P < 0.05$, Fig. 3A) in p62-knockdown and control U937 cells. We found that miR-3064-3p, one of the top expressed miRNAs, and miR-339-5p, which was the most uniformly expressed endogenous control reference gene, were downregulated in U937 cells with p62 knockdown. RT–qPCR was used to detect the expression of exosomal miRNAs in the cells, revealing that the expression levels of miR-3064-3p and miR-339-5p decreased in U937 cells with p62 knockdown, consistent with the microarray profile (Fig. 3B).

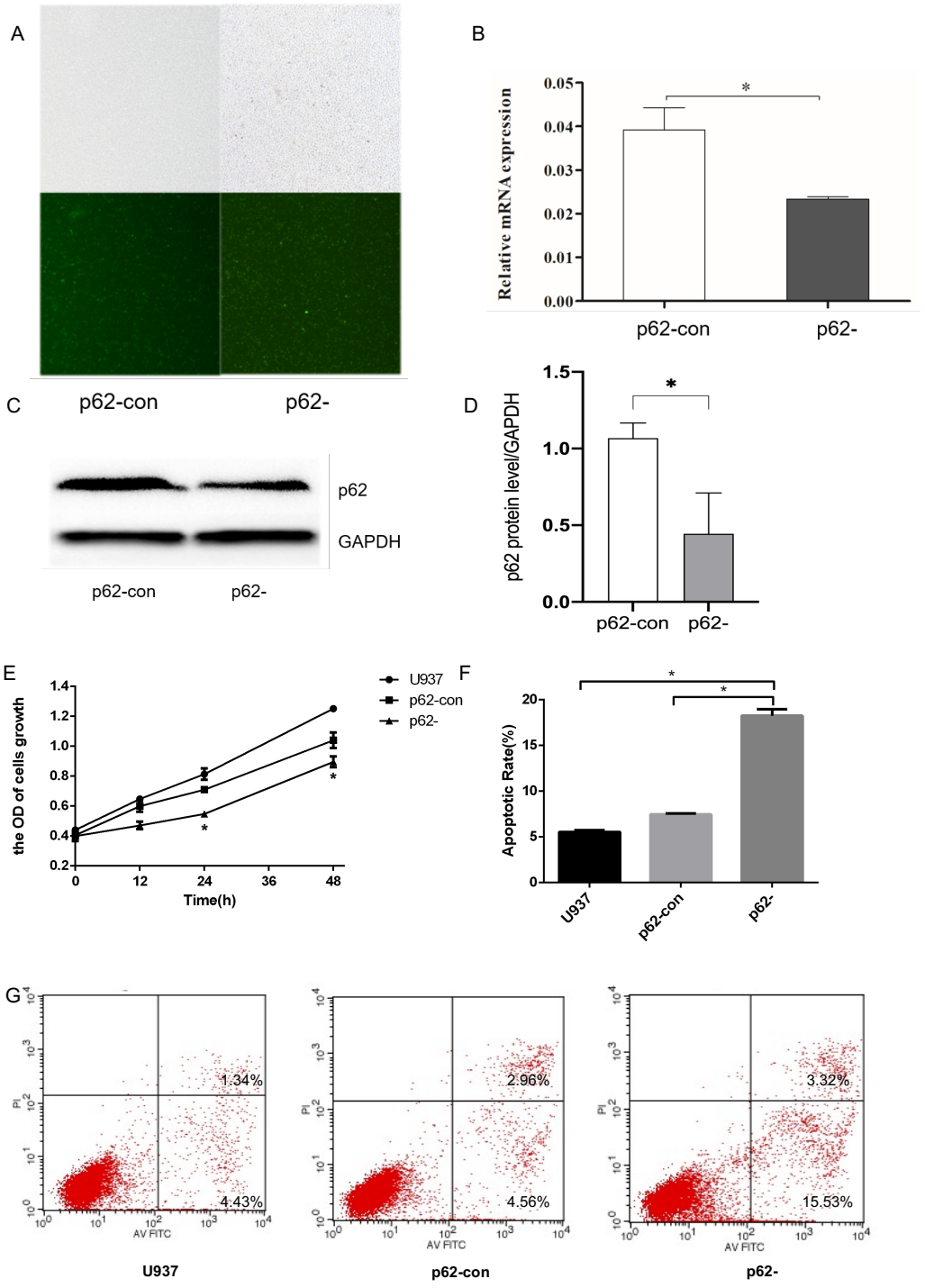

Figure 1 **The expression levels of the*p62* gene and protein in U937 cells were successfully reduced compared with controls after LV-SQSTM1-RNAi treatment.** (A) Transfection efficiency of U937 cells by fluorescence microscopy. (B) Relative mRNA expression of p62 by reverse transcription (RT)–quantitative (q)PCR. (C–D) Protein expression of p62 by western blotting. (E) Cell proliferation measured by cell counting kit (CCK)-8. (F) Apoptotic rates of cells. (G) Typical flow cytometry dot plot diagrams of cells. U937, parental cells; p62-con, U937 cells infected by an empty recombinant adenovirus vector; p62-, U937 cells with p62 knockdown. $N = 3$. Data were shown as means ± SD. $^*P < 0.05$.

Full-size DOI: 10.7717/peerj.13498/fig-1

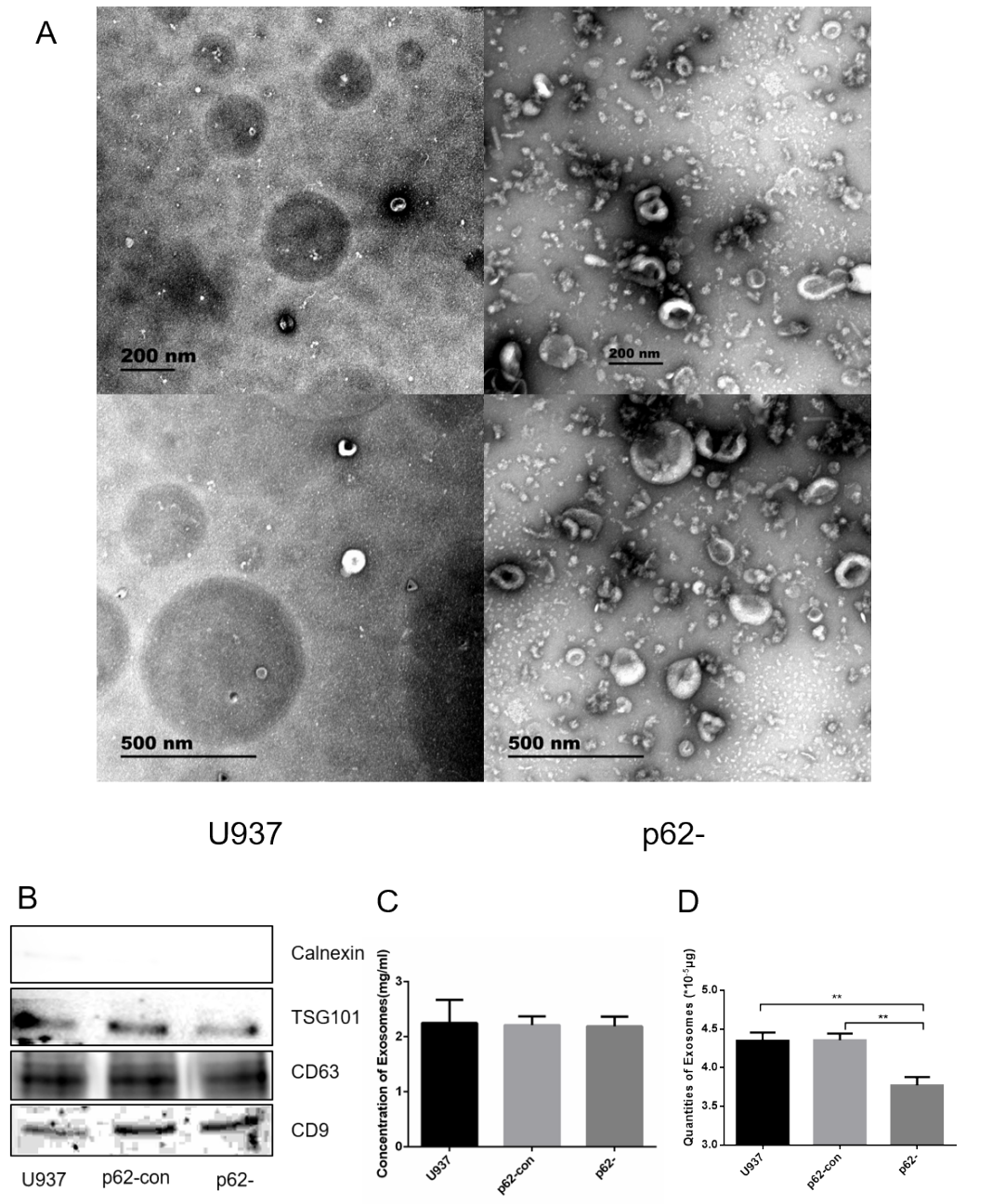

Figure 2 The exosome forms by electron microscopy after ultracentrifugation. (A) Exosomes from U937 cells with p62 knockdown and parental cells by scanning electron microscope. (B) Western blot results of exosomal protein expression from three cell lines. (C) Concentrations of exosomes in three cell lines. (D) Quantities of exosomes in three cell lines. U937, parental cells; p62-con, U937 cells infected by an empty recombinant adenovirus vector; p62-, U937 cells with p62 knockdown. $N = 3$. Data were shown as means ± SD. $^{**}P < 0.01$.

Full-size DOI: 10.7717/peerj.13498/fig-2

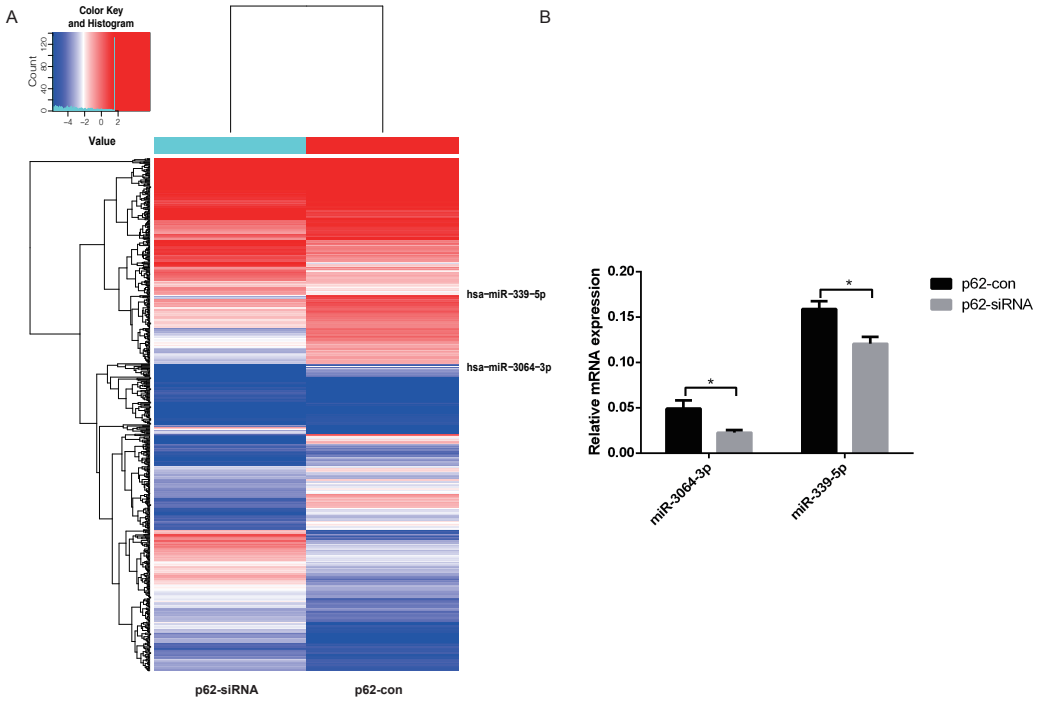

Figure 3 **The differentially expressed miRNAs in exosomes.** (A) A heat map of U937 cells (p62 knockdown and control). The red parts indicate a high expression level and blue corresponds to a low expression level. (B) Relative expression of miRNA-3064-3p and miR-339-5p. U937, parental cells; p62-con, U937 cells infected by an empty recombinant adenovirus vector; p62-, U937 cells with p62 knockdown. $N = 3$. Data were shown as means ± SD. $^*P < 0.05$.

Full-size DOI: 10.7717/peerj.13498/fig-3

GO and KEGG pathway analyses of differentially expressed miRNAs

We used GO and KEGG pathways to analyze the top 50 miRNAs that were upregulated and downregulated in p62-knockdown and control U937 cells, respectively. We focused on cellular component (CC) (Figs. 4E–4F), biological process (BP) (Figs. 4C–4D), and molecular function (MF) (Figs. 4G–4H) targeted by upregulated and downregulated genes. We found that the neuron part was the top part of gene expression in downregulated genes, including 233 genes (Fig. 4B), and that the intercellular part was the top part of upregulated genes, including 1,843 genes (Figs. 4G, 4E). According to the BP analysis, 1,460 BPs were associated with downregulated transcripts, 19 pathways were related to vesicles, 1,515 pathways were related to upregulated transcripts, and 8 pathways were related to vesicles. MF analysis revealed that 1,544 upregulated genes and 1,200 downregulated genes were involved in protein binding (Figs. 4G–4H). KEGG pathway analysis indicated that 84 pathways corresponded to upregulated transcripts, and 55 pathways corresponded to downregulated transcripts ($P < 0.05$) (Figs. 5A and 6A). For downregulated transcripts, the "TNF signaling pathway" (Pathway ID: hsa04668) that included 23 genes was most affected, followed by the "MAPK pathway" (Pathway ID: hsa04010) (Fig. 5A). As for upregulated transcripts, the "PI3K–Akt signaling pathway" (Pathway ID: hsa04151) that included 80 upregulated genes was the most enriched pathway (Fig. 6A). The miRNAs of exosomes

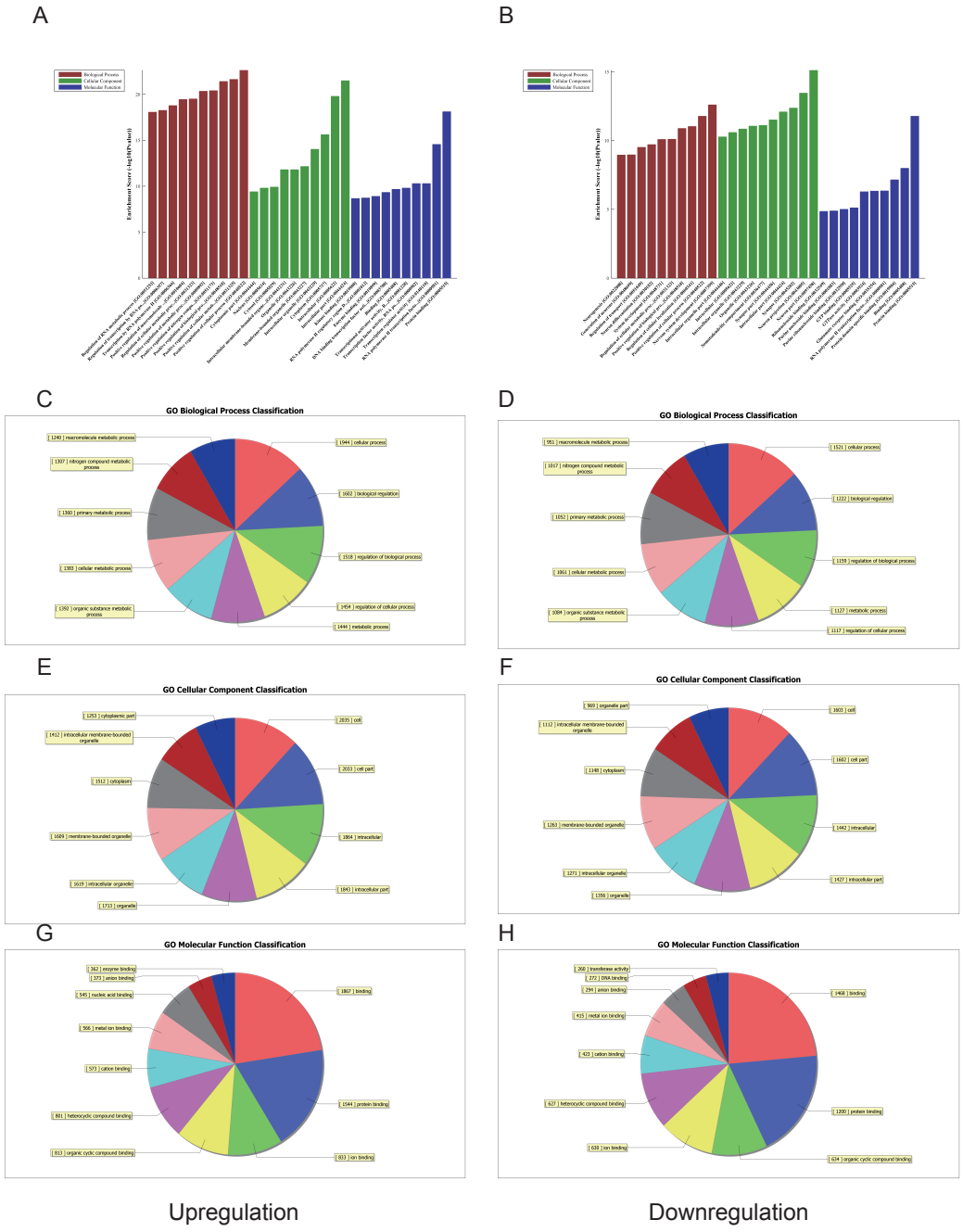

Figure 4 Gene ontology (GO) analysis of the top 50 miRNAs for upregulation and downregulation in U937 cells with p62 knockdown and controls, respectively. (A) The most highly enriched GO terms for differentially expressed transcripts for upregulation. (B) The most highly enriched GO terms for differentially expressed transcripts for downregulation. The most highly enriched GO terms for upregulated transcripts: (C) biological process (BP); (E) cellular component (CC); and (G) molecular function (MF). The most highly enriched GO terms for downregulated transcripts: (D) biological process (BP); (F) cellular component (CC); and (H) molecular function (MF).

Full-size DOI: 10.7717/peerj.13498/fig-4

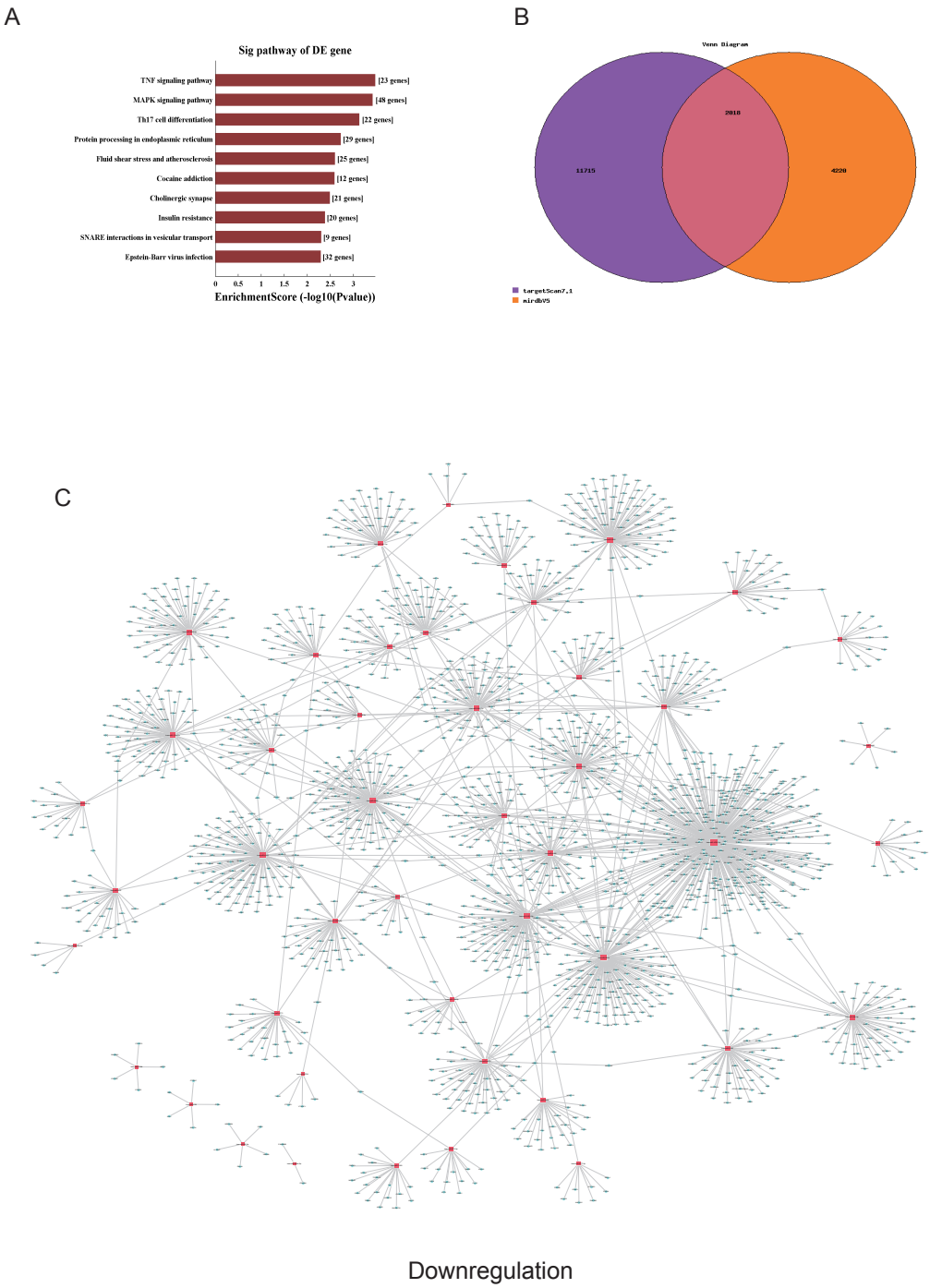

Figure 5 **Corresponding down-regulated pathways and network of miRNAs and mRNAs.** (A) Corresponding pathways of downregulation; (B) Venn diagram of miRNA co-expression in downregulation between targetscan7.1 and mirdbV5; (C) network of miRNAs and mRNAs in downregulation.
Full-size DOI: 10.7717/peerj.13498/fig-5

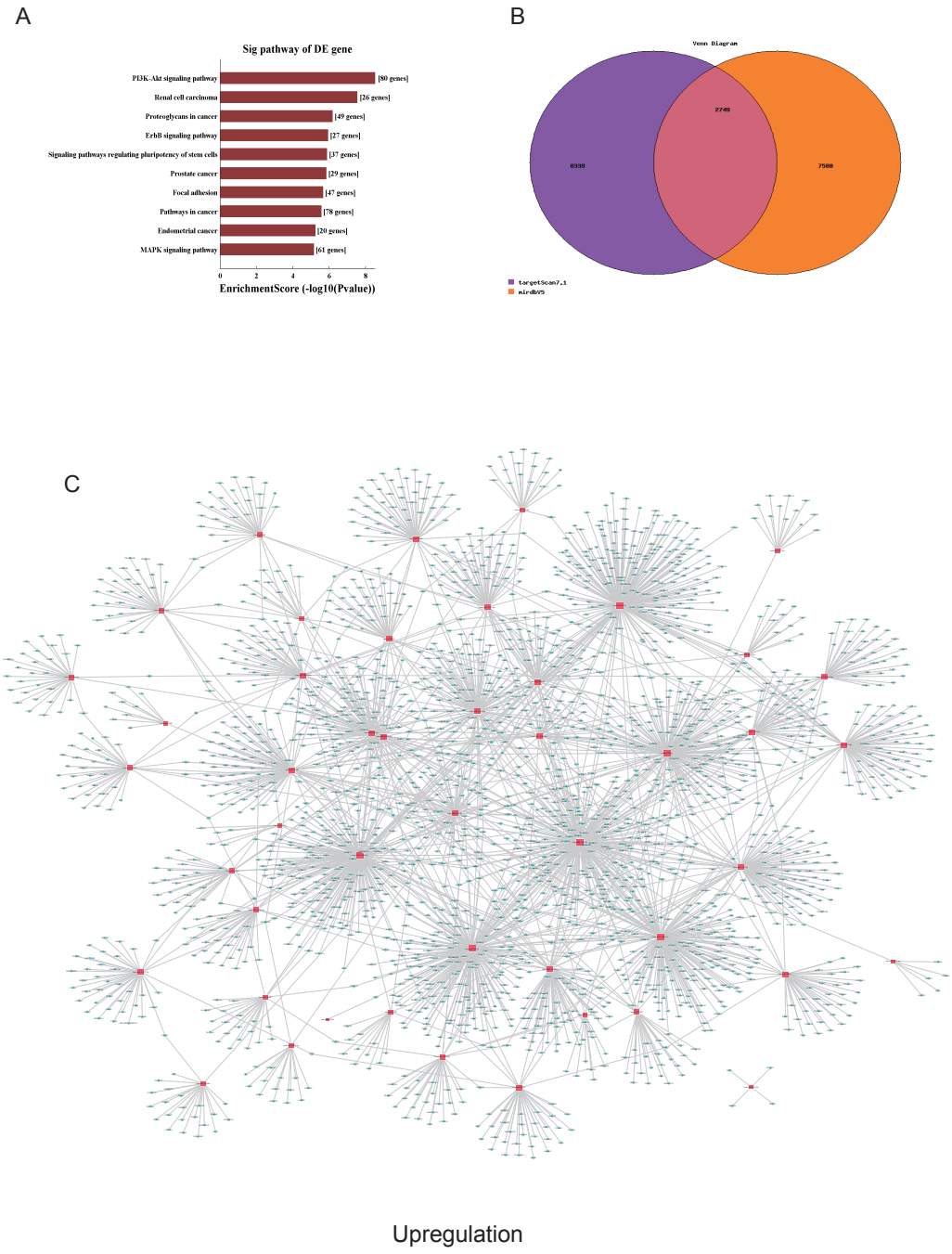

Figure 6 **Corresponding up-regulated pathways and network of miRNAs and mRNAs.** (A) Corresponding pathways of upregulation; (B) Venn diagram of miRNA co-expression in upregulation between targetscan7.1 and mirdbV5; (C) network of miRNAs and mRNAs in upregulation.

Full-size DOI: 10.7717/peerj.13498/fig-6

derived from U937 cells (p62-knockdown and controls) influenced gene expression and signaling pathways that participated in vesicle formation and AML generation (Figs. 5A and 6A).

MiRNA and mRNA networks and prediction of miRNA function

TargetScan7.1 (http://www.targetscan.org/) and mirdbV5 (http://mirdb.org/) were employed to predict the potential target genes of miRNAs. We found that 2,018 genes co-expressed with upregulated miRNAs and 2,749 genes co-expressed with downregulated miRNAs in the two databases (Figs. 5B and 6B). Besides, networks of miRNAs and mRNAs in upregulation and downregulation were shown in the Figs. 5C and 6C.

HUVEC angiogenesis

HUVECs were inoculated in Matrigel and incubated with AML exosomes for a certain period of time to determine whether exosomes from AML cells could induce HUVEC tubular differentiation *in vitro*. A CCK-8 assay was used to detect cell proliferation after 12, 24 and 48 h. The proliferation of cell lines was not statistically significant (Fig. 7A). Microscopic analysis showed that exosomes from U937 cells induced the formation of a tubular network, compared with p62-knockdown and p62-control cells (Figs. 7B–7C). By counting the node number, junction number and segment length, we found that the HUVECs with U-937 cells and exosomes generated more blood vessels ($p < 0.05$). Among the three groups of HUVECs+Exo(U937), HUVECs+Exo(p62-con) and HUVECs+Exo(p62-), the HUVECs+Exo(p62-) group grew slower than the other two groups ($p < 0.05$). In summary, the above results indicated that the fastest angiogenesis occurred in the presence of exosomes from U937 cells; the slowest angiogenesis occurred in the presence of exosomes from p62-knockdown U937 cells.

DISCUSSION

Although advances have been made in AML supportive care, prognostic risk stratification, and established therapies, patients with AML have poor long-term prognosis (*De Kouchkovsky & Abdul-Hay, 2016*). The identification of several gene mutations can guide treatment, such as PML-RARA for acute promyelocytic leukemia (APL). P62 is an autophagy receptor and a selective adaptor protein. In addition, p62 is involved in many signal transduction pathways, including the Keap1–Nrf2 pathway that plays a critical role in proteasomal degradation of ubiquitinated proteins and autophagy progression (*Liu et al., 2016*). Ser407 of the ubiquitin-associated (UBA) domain of p62 is phosphorylated by autophagy-associated protein 1 (ATG1/ULK1), followed by phosphorylation at Ser403 of the UBA domain by casein kinase 2 or TANK-binding kinase 1 that leads to p62 ubiquitination and promotes autophagic degradation (*Myeku & Figueiredo-Pereira, 2011*). The PB1 domain of p62 promotes packaging of ubiquitinated substrates by self-oligomerization and transports packaged substrates to the autophagy pathway to participate in autophagosome formation (*Ichimura et al., 2008*). P62 interacts with LC3, an autophagosome marker protein, to form a complex through its LIR domain that is degraded in autophagosomes as an autophagy-specific substrate (*Pankiv et al., 2007*). A study has

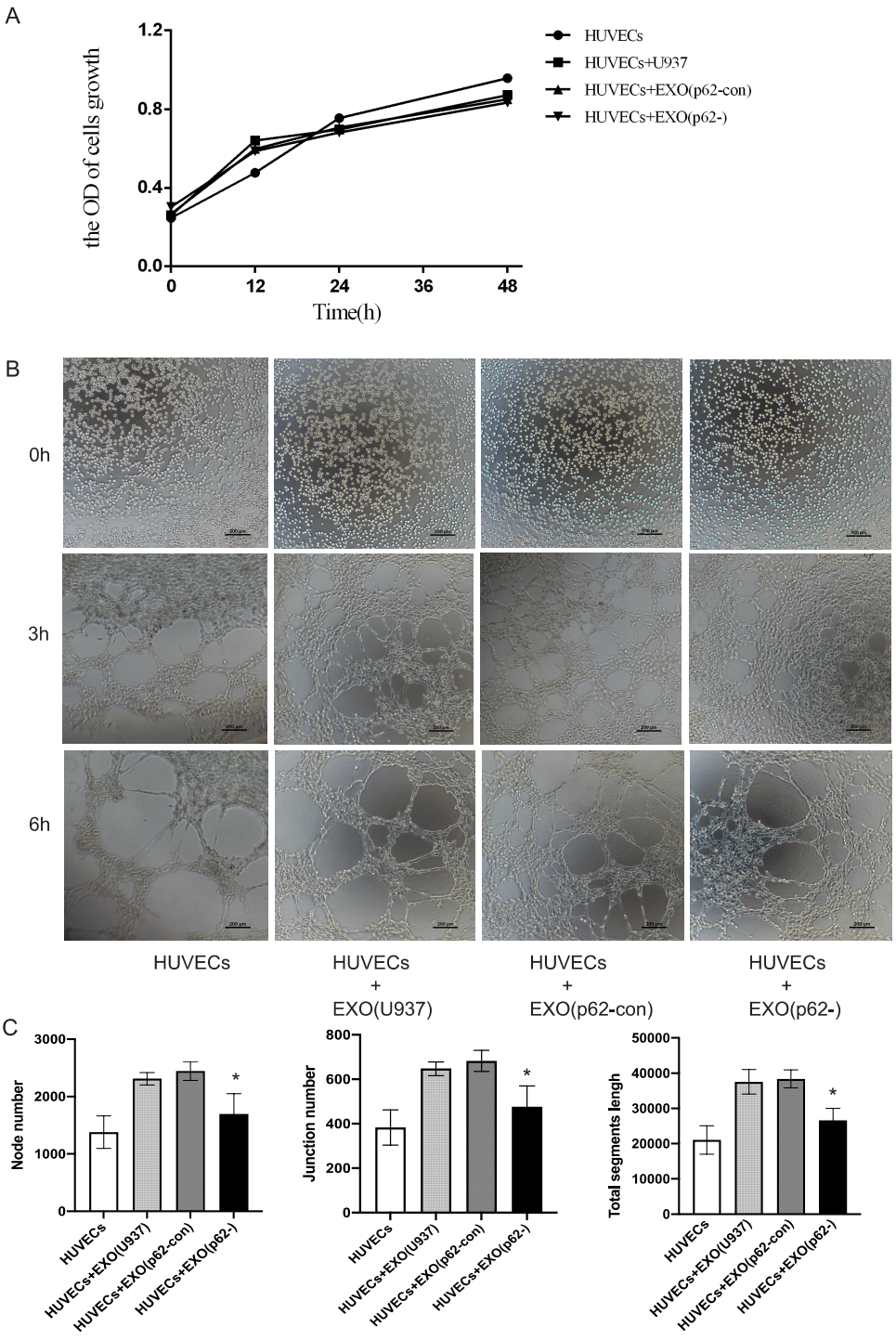

Figure 7 HUVECs were co-cultured with exosomes secreted by AML cells. (A) A cell counting kit (CCK)-8 assay was used to detect cell proliferation after 12, 24 and 48 h. The proliferation of cell lines was not statistically significant; (B) 0, 3 and 6 h to detect HUVEC angiogenesis. We found the exosomes of U937 cells can promote the angiogenesis of HUVECs. (C) Quantitative results of 6 h angiogenesis assay. EXO, exosomes; HUVECs, human umbilical vein endothelial cells; AML, acute myeloid leukemia; U937, parental cells; p62-con, U937 cells infected by an empty recombinant adenovirus vector; p62-, U937 cells with p62 knockdown. $N = 3$. Data were shown as means ± SD. $^{*}P < 0.05$.

Full-size DOI: 10.7717/peerj.13498/fig-7

shown that mutations in SQSTM1, which codes for p62, are a causative factor in Paget disease of bone, as well as amyotrophic lateral sclerosis and frontotemporal dementia (*Le Ber et al., 2013*). Abnormal amplification and phosphorylation of p62/SQSTM1 have been implicated in tumor progression and resistance therapy, such as in hepatocellular carcinoma (*Saito et al., 2016*), and platinum-resistant cells of high-grade serous ovarian cancer (*Nguyen et al., 2017*). P62/SQSTM1 upregulation promotes granulocytic differentiation and survival of AML cells through a mechanism that depends on NF-κB activation (*Trocoli et al., 2014*).

Accumulating evidence indicates that exosomes in tumors are oncogenic. Crosstalk between bone marrow tumors and endothelial cells can affect tumor progression in hematological tumors, and exosomes containing miRNAs are crucial in bone marrow angiogenesis promotion in hematological tumors. By delivering miR-365, exosomes can mediate the horizontal transfer of drug resistance in chronic myeloid leukemia cells (*Saito et al., 2016*). K562 cells secrete exosomes containing miR-92a, which can enhance angiogenesis; miR-135b, which targets inhibitory hypoxia-inducible factor 1 angiogenesis, also enhances exocytosis secretion by multiple myeloma cells (*Ohyashiki, Umezu & Ohyashiki, 2016*).

In our study, p62 knockdown in U937 cells inhibited cell proliferation and promoted apoptosis ($P < 0.05$). We used microarray technology to study the expression patterns of exosomal miRNAs derived from two U937 cell lines to further explore the relationship between exosomal miRNAs and p62. We identified 2,080 miRNAs, including 215 upregulated and 208 downregulated miRNAs in p62-knockdown U937 cells. To further validate microarray analysis results, we performed RT–qPCR to validate the downregulated expression of miR-3064-3p and miR-339-5p in the same series of samples. Our future studies will involve identification of other miRNAs whose expression was the highest in our microarray results. The RT–qPCR results were consistent with those obtained from microarray analysis. In addition, KEGG pathway analysis revealed that 84 pathways corresponded to upregulated transcripts, and 55 pathways corresponded to downregulated transcripts. For the downregulated transcripts, the most affected pathway was the "TNF signaling pathway" (Pathway ID: hsa04668), followed by the "MAPK pathway" (Pathway ID: hsa04010). As for upregulated transcripts, the "PI3K–Akt signaling pathway" (Pathway ID: hsa04151) was the most enriched pathway.

We constructed a miRNA–mRNA correlation network that displayed 2,749 upregulated and 2,018 downregulated co-expressed genes in two databases. According to previous research, vascular endothelial growth factor A (VEGFA), VEGFC, GATA-binding protein 4 (*Jia et al., 2018*), matrix metallopeptidase 2 (*Sun et al., 2010*), and zinc finger protein (*Li et al., 2016*), were involved in cell angiogenesis in the co-expression network. These results negatively correlated with those of hsa-miR-3064-3p and hsa-miR-339-5p in our profiles. Furthermore, hsa-miR-3622a-5p and hsa-miR-3064-3p displayed significant negative correlations with the Grb2-associated regulators of mitogen-activated protein kinase (MAPK) 1 and MAPK6, which participate in the MAPK signaling pathway. These findings indicate that hsa-miR-3064-3p, hsa-miR-339-5p, hsa-miR-3622a-5p, and their

co-expressed coding genes in the MAPK signaling pathway may play a significant role in the angiogenesis of AML cells.

Although AML cells secrete angiogenic factors to remodel the vascular system and gain chemoresistance, anti-angiogenic drugs are generally ineffective in AML treatment. *Wang et al. (2019)* found that exosomes secreted by AML cells can enhance glycolysis-mediated vascular remodeling and chemoresistance. According to previous reports, wogonoside inhibits angiogenesis in solid tumors by blocking the JAK2-STAT3 pathway and inhibiting the development of hematologic malignancies in AML (*Lin et al., 2019*). To further validate the exosome and angiogenesis results in AML, we grew HUVECs in the presence of exosomes derived from parental U937 cells, p62-knockdown U937 cells, and p62-control cells. We found that angiogenesis was fastest in the presence of U937 exosomes and slowest in the presence of p62-knockdown U937 exosomes. This finding illustrates that exosomes derived from AML cells play an important role in the angiogenesis of HUVECs.

CONCLUSIONS

In conclusion, after a detailed examination of miRNA expression in exosomes derived from AML cells, we found that hsa-miR-3064-3p and hsa-miR-339-5p displayed downregulated expression in p62-knockdown cells, compared with control cells. In addition, we demonstrated that several differentially expressed exosomal miRNAs were closely related to multiple GO items and pathways involved in carcinogenesis, indicating that exosomal miRNAs play a key role in AML pathogenesis. This information may aid the development of potential biomarkers for diagnosis and prognosis of AML progression. In the present study, we also found that exosomes derived from AML cells promoted angiogenesis. However, the relationship between exosomal miRNAs and angiogenesis needs to be further investigated. These findings support the notion that promising new treatment strategies may be developed against AML, based on exosomal miRNA analysis.

ADDITIONAL INFORMATION AND DECLARATIONS

Funding

This project is supported by the Scientific research project of the Education Department of Liaoning Province (2019 64). The funders had no role in study design, data collection and analysis, decision to publish, or preparation of the manuscript.

Grant Disclosures

The following grant information was disclosed by the authors:
Scientific research project of the Education Department of Liaoning Province (2019 64).

Competing Interests

The authors declare there are no competing interests.

Author Contributions

- Chuan Li conceived and designed the experiments, performed the experiments, prepared figures and/or tables, authored or reviewed drafts of the article, and approved the final draft.
- Xinyi Long conceived and designed the experiments, performed the experiments, prepared figures and/or tables, and approved the final draft.
- Peiqi Liang analyzed the data, prepared figures and/or tables, and approved the final draft.
- Zhuogang Liu conceived and designed the experiments, analyzed the data, prepared figures and/or tables, authored or reviewed drafts of the article, and approved the final draft.
- Chen Wang analyzed the data, prepared figures and/or tables, and approved the final draft.
- Rong Hu conceived and designed the experiments, prepared figures and/or tables, authored or reviewed drafts of the article, and approved the final draft.

Microarray Data Deposition

The following information was supplied regarding the deposition of microarray data:

The data is available at GEO: GSE192628.
https://www.ncbi.nlm.nih.gov/geo/query/acc.cgi?acc=GSE192628.

Data Availability

The following information was supplied regarding data availability:

The data are available in the Supplementary Files.

Supplemental Information

Supplemental information for this article can be found online at http://dx.doi.org/10.7717/peerj.13498#supplemental-information.

REFERENCES

Agarwal V, Bell GW, Nam JW, Bartel DP. 2015. Predicting effective microRNA target sites in mammalian mRNAs. *Elife* **4**:e05005 DOI 10.7554/eLife.05005.

Aslan C, Maralbashi S, Salari F, Kahroba H, Sigaroodi F, Kazemi T, Kharaziha P. 2019. Tumor-derived exosomes: implication in angiogenesis and antiangiogenesis cancer therapy. *Journal of Cellular Physiology* **234**:16885–16903 DOI 10.1002/jcp.28374.

Burnett A, Wetzler M, Lowenberg B. 2011. Therapeutic advances in acute myeloid leukemia. *Journal of Clinical Oncology* **29**:487–494 DOI 10.1200/JCO.2010.30.1820.

Chen Y, Wang X. 2020. miRDB: an online database for prediction of functional microRNA targets. *Nucleic Acids Research* **48**:D127–D131 DOI 10.1093/nar/gkz757.

De Kouchkovsky I, Abdul-Hay M. 2016. Acute myeloid leukemia: a comprehensive review and 2016 update. *Blood Cancer Journal* **6**:e441 DOI 10.1038/bcj.2016.50.

Haouas H. 2014. Angiogenesis and acute myeloid leukemia. *Hematology* **19**:311–323 DOI 10.1179/1607845413Y.0000000139.

Hornick NI, Doron B, Abdelhamed S, Huan J, Harrington CA, Shen R, Cambronne XA, Chakkaramakkil Verghese S, Kurre P. 2016. AML suppresses hematopoiesis by releasing exosomes that contain microRNAs targeting c-MYB. *Science Signaling* **9**:ra88 DOI 10.1126/scisignal.aaf2797.

Ichimura Y, Kumanomidou T, Sou YS, Mizushima T, Ezaki J, Ueno T, Kominami E, Yamane T, Tanaka K, Komatsu M. 2008. Structural basis for sorting mechanism of p62 in selective autophagy. *Journal of Biological Chemistry* **283**:22847–22857 DOI 10.1074/jbc.M802182200.

Jia W, Wu W, Yang D, Xiao C, Huang M, Long F, Su Z, Qin M, Liu X, Zhu YZ. 2018. GATA4 regulates angiogenesis and persistence of inflammation in rheumatoid arthritis. *Cell Death & Disease* **9**:503 DOI 10.1038/s41419-018-0570-5.

Komatsu M, Kageyama S, Ichimura Y. 2012. p62/SQSTM1/A170: physiology and pathology. *Pharmacological Research* **66**:457–462 DOI 10.1016/j.phrs.2012.07.004.

Le Ber I, Camuzat A, Guerreiro R, Bouya-Ahmed K, Bras J, Nicolas G, Gabelle A, Didic M, De Septenville A, Millecamps S, Lenglet T, Latouche M, Kabashi E, Campion D, Hannequin D, Hardy J, Brice A, French C, Genetic Research Network on FF-A. 2013. SQSTM1 mutations in French patients with frontotemporal dementia or frontotemporal dementia with amyotrophic lateral sclerosis. *JAMA Neurology* **70**:1403–1410 DOI 10.1001/jamaneurol.2013.3849.

Li HS, Jin J, Liang X, Matatall KA, Ma Y, Zhang H, Ullrich SE, King KY, Sun SC, Watowich SS. 2016. Loss of c-Kit and bone marrow failure upon conditional removal of the GATA-2 C-terminal zinc finger domain in adult mice. *European Journal of Haematology* **97**:261–270 DOI 10.1111/ejh.12719.

Lin B, Zhao K, Yang D, Bai D, Liao Y, Zhou Y, Yu Z, Yu X, Guo Q, Lu N. 2019. Wogonoside impedes the progression of acute myeloid leukemia through inhibiting bone marrow angiogenesis. *Journal of Cellular Physiology* **234**:1913–1924 DOI 10.1002/jcp.27067.

Liu WJ, Ye L, Huang WF, Guo LJ, Xu ZG, Wu HL, Yang C, Liu HF. 2016. p62 links the autophagy pathway and the ubiqutin-proteasome system upon ubiquitinated protein degradation. *Cellular & Molecular Biology Letters* **21**:29 DOI 10.1186/s11658-016-0031-z.

Myeku N, Figueiredo-Pereira ME. 2011. Dynamics of the degradation of ubiquitinated proteins by proteasomes and autophagy: association with sequestosome 1/p62. *Journal of Biological Chemistry* **286**:22426–22440 DOI 10.1074/jbc.M110.149252.

Nguyen EV, Huhtinen K, Goo YA, Kaipio K, Andersson N, Rantanen V, Hynninen J, Lahesmaa R, Carpen O, Goodlett DR. 2017. Hyper-phosphorylation of sequestosome-1 distinguishes resistance to cisplatin in patient derived high grade serous ovarian cancer cells. *Molecular & Cellular Proteomics* **16**:1377–1392 DOI 10.1074/mcp.M116.058321.

Nguyen TD, Shaid S, Vakhrusheva O, Koschade SE, Klann K, Tholken M, Baker F, Zhang J, Oellerich T, Surun D, Derlet A, Haberbosch I, Eimer S, Osiewacz HD, Behrends C, Munch C, Dikic I, Brandts CH. 2019. Loss of the selective autophagy

receptor p62 impairs murine myeloid leukemia progression and mitophagy. *Blood* **133**:168–179 DOI 10.1182/blood-2018-02-833475.

Ohyashiki JH, Umezu T, Ohyashiki K. 2016. Exosomes promote bone marrow angiogenesis in hematologic neoplasia: the role of hypoxia. *Current Opinion in Hematology* **23**:268–273 DOI 10.1097/MOH.0000000000000235.

Pankiv S, Clausen TH, Lamark T, Brech A, Bruun JA, Outzen H, Overvatn A, Bjorkoy G, Johansen T. 2007. p62/SQSTM1 binds directly to Atg8/LC3 to facilitate degradation of ubiquitinated protein aggregates by autophagy. *Journal of Biological Chemistry* **282**:24131–24145 DOI 10.1074/jbc.M702824200.

Patel JP, Gonen M, Figueroa ME, Fernandez H, Sun Z, Racevskis J, Van Vlierberghe P, Dolgalev I, Thomas S, Aminova O, Huberman K, Cheng J, Viale A, Socci ND, Heguy A, Cherry A, Vance G, Higgins RR, Ketterling RP, Gallagher RE, Litzow M, van den Brink MR, Lazarus HM, Rowe JM, Luger S, Ferrando A, Paietta E, Tallman MS, Melnick A, Abdel-Wahab O, Levine RL. 2012. Prognostic relevance of integrated genetic profiling in acute myeloid leukemia. *New England Journal of Medicine* **366**:1079–1089 DOI 10.1056/NEJMoa1112304.

Saito T, Ichimura Y, Taguchi K, Suzuki T, Mizushima T, Takagi K, Hirose Y, Nagahashi M, Iso T, Fukutomi T, Ohishi M, Endo K, Uemura T, Nishito Y, Okuda S, Obata M, Kouno T, Imamura R, Tada Y, Obata R, Yasuda D, Takahashi K, Fujimura T, Pi J, Lee MS, Ueno T, Ohe T, Mashino T, Wakai T, Kojima H, Okabe T, Nagano T, Motohashi H, Waguri S, Soga T, Yamamoto M, Tanaka K, Komatsu M. 2016. p62/Sqstm1 promotes malignancy of HCV-positive hepatocellular carcinoma through Nrf2-dependent metabolic reprogramming. *Nature Communications* **7**:12030 DOI 10.1038/ncomms12030.

Short NJ, Rytting ME, Cortes JE. 2018. Acute myeloid leukaemia. *Lancet* **392**:593–606 DOI 10.1016/S0140-6736(18)31041-9.

Skog J, Wurdinger T, Rijn Svan, Meijer DH, Gainche L, Sena-Esteves M, Curry Jr WT, Carter BS, Krichevsky AM, Breakefield XO. 2008. Glioblastoma microvesicles transport RNA and proteins that promote tumour growth and provide diagnostic biomarkers. *Nature Cell Biology* **10**:1470–1476 DOI 10.1038/ncb1800.

Staudt D, Murray HC, McLachlan T, Alvaro F, Enjeti AK, Verrills NM, Dun MD. 2018. Targeting oncogenic signaling in mutant FLT3 acute myeloid leukemia: the path to least resistance. *International Journal of Molecular Sciences* **19(10)**:3198 DOI 10.3390/ijms19103198.

Sun HY, Wei SP, Xu RC, Xu PX, Zhang WC. 2010. Sphingosine-1-phosphate induces human endothelial VEGF and MMP-2 production via transcription factor ZNF580: novel insights into angiogenesis. *Biochemical and Biophysical Research Communications* **395**:361–366 DOI 10.1016/j.bbrc.2010.04.019.

Trocoli A, Bensadoun P, Richard E, Labrunie G, Merhi F, Schläfli AM, Brigger D, Souquere SPG, Pasquet JM, Soubeyran P, Reiffers J, Ségal-Bendirdjian E, Tschan MP, Djavaheri-Mergny M. 2014. p62/SQSTM1 upregulation constitutes a survival mechanism that occurs during granulocytic differentiation of acute myeloid leukemia cells. *Cell Death & Differentiation* **21**:1852–1861 DOI 10.1038/cdd.2014.102.

Wang B, Wang X, Hou D, Huang Q, Zhan W, Chen C, Liu J, You R, Xie J, Chen P, Huang H. 2019. Exosomes derived from acute myeloid leukemia cells promote chemoresistance by enhancing glycolysis-mediated vascular remodeling. *Journal of Cellular Physiology* **234**:10602–10614 DOI 10.1002/jcp.27735.

Xie M, Lu C, Wang J, McLellan MD, Johnson KJ, Wendl MC, McMichael JF, Schmidt HK, Yellapantula V, Miller CA, Ozenberger BA, Welch JS, Link DC, Walter MJ, Mardis ER, Dipersio JF, Chen F, Wilson RK, Ley TJ, Ding L. 2014. Age-related mutations associated with clonal hematopoietic expansion and malignancies. *Nature Medicine* **20**:1472–1478 DOI 10.1038/nm.3733.